Polymer Chemistry

ROYAL SOCIETY OF CHEMISTRY

PAPER

View Article Online
View Journal | View Issue

Cite this: *Polym. Chem.*, 2025, **16**, 1669

Biocompatible two-dimensional platelets with tunable sizes from polycarbonate-based block copolymers†

Chuanqi Zhao,‡[a] Hannah Schnicke, ‡[a] J. Diego Garcia-Hernandez,[a] Jiandong Cai,[a] Yifan Zhang,§[a] Charlotte E. Boott *[c] and Ian Manners¶[a,b]

Two-dimensional (2D) nanoparticles have received considerable attention due to their versatile applications ranging from catalysis, optoelectronics to nanomedicine. However, it remains challenging to access size tunable flat nanostructures with spatially tailored chemistries. The seeded-growth method, "living" crystallization-driven self-assembly (CDSA) has emerged as a promising approach for preparing well-defined 1D and 2D core–shell micellar assemblies from crystallizable block copolymers (BCPs). Nevertheless, the development of biocompatible aliphatic polycarbonates, such as poly(trimethylene carbonate) (PTMC), as core-forming blocks for CDSA is considerably less explored and represents a key challenge due to their low crystallinity. Herein, we report the development of poly(dimethyltrimethylene carbonate) (PDTC) as a crystallizable core-forming block through the introduction of side chains to PTMC. The BCPs containing crystallizable PDTC were shown to undergo living CDSA to prepare uniform and size-controlled 2D platelets. In addition, uniform segmented platelets with spatially localized coronal chemistries were successfully constructed. The colloidal stability of the platelets in aqueous solution allowed for an assessment of their toxicity toward healthy WI-38 and cancerous U-87 MG cells. These studies reveal that PDTC nanostructures exhibit no discernible cytotoxicity and excellent biocompatibility, indicating great potential for biomedical applications.

Received 23rd January 2025,
Accepted 25th February 2025

DOI: 10.1039/d5py00078e

rsc.li/polymers

Introduction

Two-dimensional (2D) nanostructures have been extensively studied in the fields of catalysis,[1,2] sensing,[3,4] optoelectronics,[5–8] and biomedical materials.[9,10] Recently, considerable attention has been devoted to the use of 2D nanostructures in biomedical applications due to their prolonged circulation times in the bloodstream, reduced accumulation in the liver, and reduced immune recognition.[11–15] However, the controlled synthesis of biocompatible 2D nanostructures with predictable morphologies, sizes, and compositions is challenging.[16,17]

Crystallization-driven self-assembly (CDSA) enables amphiphilic block copolymers (BCPs) with a crystalline core-forming block to drive the solution self-assembly of low curvature morphologies, such as one-dimensional (1D) nanofibers and 2D platelets.[17] Using this approach, 2D platelets are preferentially formed from crystalline–coil BCPs with block ratios close to 1 : 1 or by tuning the solvent ratio to facilitate crystallization.[4,18–26] The size of the 2D nanoparticles synthesized by CDSA can be controlled using a seeded-growth approach, termed 'living' CDSA.[21,26–33] This versatile and robust method has been used to prepare a wide range of well-defined and complex 2D platelets with tailored coronal chemistries and modular multifunctionality, including tracking capabilities and cargo encapsulation.[11,13,14,33,34] To date, a range of biocompatible and biodegradable crystalline core-forming blocks have been shown to form 2D platelets by living CDSA. These include poly(L-lactide) (PLLA),[8,18,35,36] poly(ε-caprolactone) (PCL)[26,34,37–41] and poly(*p*-dioxanone) (PPDO).[20]

Aliphatic polycarbonates have been widely explored as a promising class of materials for biomedical applications due to their low inherent toxicity, biodegradability, biocompatibil-

[a]*Department of Chemistry, University of Victoria, Victoria, BC V8 W 3 V6, Canada*
[b]*Centre for Advanced Materials and Related Technology (CAMTEC), University of Victoria, 3800 Finnerty Rd, Victoria, BC, V8P 5C2, Canada*
[c]*Department of Chemistry and Materials Innovation Factory, University of Liverpool, Liverpool, L7 3NY, UK. E-mail: c.boott@liverpool.ac.uk*

†Electronic supplementary information (ESI) available. See DOI: https://doi.org/10.1039/d5py00078e

‡These authors contributed equally.

§Present address: Key Laboratory of Photochemistry, CAS Research/Education Center for Excellence in Molecular Sciences, Institute of Chemistry, Chinese Academy of Sciences, Beijing 100190, China.

¶Deceased December 3rd, 2023.

ity and slow biodegradation times compared to PLLA analogs.[42–44] Among the synthetic aliphatic polycarbonates reported in the literature, poly(trimethylene carbonate) (PTMC) has been extensively explored as a drug delivery device and scaffold for tissue engineering.[45–48] PTMC is an excellent candidate due to its *in vivo* biodegradation behavior, biocompatibility, high flexibility and toughness.[47,48] However, PTMC is a predominantly amorphous polymer with a low glass transition temperature (T_g = *ca.* −20 °C) and is only semi-crystalline in the stretched state.[49,50] Its amorphous nature limits its application as a crystalline core-forming block for CDSA. Changes to the chemical structure have been demonstrated to allow for the crystallization of a previously amorphous core-forming block.[51] Previously, we have identified a PTMC derivative, poly(fluorene trimethylene carbonate) (PFTMC), as an excellent crystalline core-forming block for use in living CDSA to form a wide variety of functional nanofibers.[50,52–58] Recently, we have reported low dispersity PFTMC-*b*-PDMAEMA (poly(2-(dimethylamino)ethyl methacrylate) nanofibers of controlled length (22–1300 nm) and demonstrated their length-dependent antimicrobial activity as well as their antibiotic and nucleic acid delivery capabilities.[55–58] Additional properties such as stability, enzymatic degradability and low inherent toxicity show the excellent biocompatibility of these nanofibers.[50,55] Despite these promising properties, the hydrolytic biodegradation product of PFTMC, 9*H*-fluorene-9,9-dimethanol, revealed increased cytotoxicity with IC_{50} values (the amount of material required to inhibit cell viability by 50%) of 1.01 mM and 0.45 mM against HeLa and WI-38 cell lines, respectively.[50] Next to well controlled 1D nanofibers, there is only one example of polydisperse 2D nanoribbons of PFTMC-*b*-poly(ethylene glycol) (PEG) upon increasing the core-to-corona ratio to 1 : 2.[50] However, to date, no size controlled 2D nanostructures prepared by living CDSA with a polycarbonate-based core-forming block have been reported. Therefore, developing a new crystalline polycarbonate-based core-forming block for living CDSA to yield precisely controlled 2D platelets with less harmful biodegradation products is the inspiration for the present work. We envisioned that alternative polycarbonate-based crystalline core-forming blocks could be developed through the introduction of different side groups to PTMC to improve its crystallinity (Fig. 1).

Herein, we investigated the steric hindrance effect of different side groups of PTMC derivatives (*e.g.* methyl, ethyl, *n*-propyl, *n*-butyl, cyclopropane and cyclobutane groups) on the homopolymer crystallinity. Poly(2,2-dimethyltrimethylene carbonate) (PDTC) showed improved crystallinity over the PTMC derivatives and was explored as a core-forming block for CDSA. Living CDSA of amphiphilic BCPs of PDTC-*b*-PEG was performed and it yielded precisely controlled 2D platelets. Additionally, well-defined segmented 2D platelets with spatially localized coronal chemistries were obtained *via* sequential living CDSA from PDTC-based BCPs with different corona functionalities. As the hydrophilic PEG corona provides colloidal stability of the nanostructures in aqueous media, the toxicity of the 2D platelets towards WI-38 and U-87 MG cells

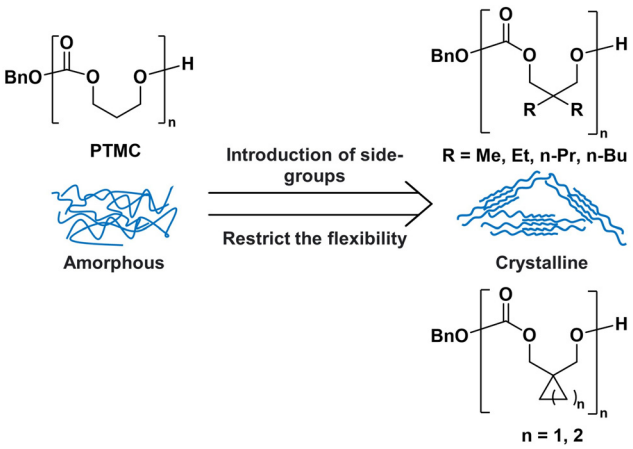

Fig. 1 Schematic illustration of increasing the crystallinity of poly(trimethylene carbonate) (PTMC) derivatives with different side groups.

was evaluated. These experiments revealed no discernible cytotoxicity of the nanomaterials towards either cell line, showing their great potential for further biomedical applications such as drug delivery vehicles.

Results and discussion

Crystallization behavior of polycarbonate homopolymers with different side groups

Homopolymers of PTMC derivatives were prepared *via* ring opening polymerization (ROP). The six-membered aliphatic carbonate monomers were obtained from their corresponding diols (Fig. S1–S6†). Changes to the chemical structure of the diols allow us to introduce different side chains or cyclic groups into the backbone of the six-membered aliphatic carbonate monomers and homopolymers, respectively.

The number-average degree of polymerization (DP_n) of each polymer was determined by ^{1}H NMR spectroscopy (Table 1, Table S1 and Fig. S7A–S12A†) while gel permeation chromatography (GPC) analysis revealed low dispersity values ($Đ_m$) between 1.14 and 1.30 (Table 1, Table S1 and Fig. S7B–S12B†). The crystallinity of each homopolymer was investigated by differential scanning calorimetry (DSC). DSC revealed that different side chains have a significant influence on the T_g and melting transition temperature (T_m) of the polycarbonate analogs (Table 1, Table S1 and Fig. S7C–S12C and S13†). All PTMC derivatives with different side chain lengths show increased T_g values in comparison with unsubstituted PTMC (T_g = −19 °C), while the dimethyl-substituted polycarbonate (PDTC) showed the highest T_g value of 27 °C. However, with increasing side chain length, the T_g values decrease from 27 °C to −11 °C. This phenomenon is well known, as longer alkyl chains decrease the frictional interactions between the polymer chains resulting in lower T_g values.[59] Also, we introduced cyclic side groups such as cyclopropane and cyclobutene; the former exhibited an increased T_g value of 51 °C,

Table 1 Synthesis of polycarbonate homopolymers *via* organocatalytic ROP

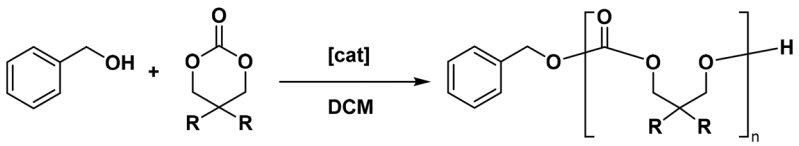

R	Polymer[c]	M_n [d] (g mol^{-1})	$Đ_m$ [d]	T_m [e] (°C)	T_c [e] (°C)	T_g [e] (°C)
H[a]	$PTMC_{65}$	8630	1.16	—	—	−19
Me[a]	$PDTC_{88}$	14 550	1.30	94, 109[f]	98	27
Et[a]	$PDEC_{35}$	7780	1.13	84, 95[f]	—	−6
n-Pr[b]	$PDPC_{58}$	11 400	1.16	104	—	−7
n-Bu[b]	$PDBC_{26}$	5210	1.14	47	—	−11

[a] TU (*N*-(3,5-trifluoromethyl)phenyl-*N*-cyclohexyl-thiourea) was used as the catalyst, and DBU (1,8-diazabicyclo[5.4.0]undec-7-ene) was used as the base for the polymerization. [b] DPP was used as the catalyst for the preparation. [c] Determined by ^{1}H NMR spectroscopy. [d] Determined by GPC *versus* polystyrene standards. [e] Determined from the DSC thermogram. [f] Two temperatures indicate two distinct peaks in the DSC data, suggesting the coexistence of two crystal forms.

while the latter showed no T_g value due to annealing of the homopolymer sample (Table S1†). Additionally, crystallization points at 87 °C and 175 °C were observed for the cyclopropane and cyclobutene derivatives, respectively (Table S1†). Notably, these homopolymers do not follow the same trend as the PTMC derivatives with increasing side chain length, and due to their poor solubility, they were not studied further (Fig. S14†). These findings reveal that the introduction of side chains and cyclic side groups successfully restricts polymer backbone flexibility and improves their crystallinity.[60] PDTC was the only PTMC derivative with side chains that exhibited a T_c of 98 °C. This suggests that PDTC crystallizes more readily than the other PTMC derivatives with different side chains as the DSC experiment for each homopolymer was performed under the same conditions. Due to its improved crystallinity, PDTC was chosen as the core-forming block for the following living CDSA studies. In addition, complementary CDSA studies with PDEC as the core-forming block were performed to explore the effect of side chain length on the self-assembly properties.

Synthesis and self-assembly of PDTC-*b*-PEG and PDEC-*b*-PEG block copolymers

To investigate the effect of block ratio on the CDSA of PDTC-*b*-PEG and PDEC-*b*-PEG polymers, a series of well-defined BCPs with different core-forming block lengths were prepared by ROP (Table 2 and Table S2†). Due to the living characteristic of the ROP, increasing amounts of the cyclic carbonate monomers DTC and ETC yielded higher DP_n for the core forming blocks, respectively (Fig. S15–S23†). For each BCP, the DP_n of the PDTC and PDEC blocks was determined using ^{1}H NMR spectroscopy, while GPC analysis revealed low dispersity values ($Đ_m$) below 1.1. These low dispersity BCPs are ideal for studying their self-assembly process in solution as they should yield morphologically pure nanoparticles.[61,62]

Next, the solution state self-assembly behavior of each BCP was investigated by attempting to form micelles *via* homogeneous nucleation in mixtures of MeOH and THF (Fig. 2). Under these conditions, MeOH acts as a selective solvent for the PEG block to promote self-assembly, while a small amount

Table 2 Synthesis of PDTC-*b*-PEG BCPs *via* organocatalytic ROP

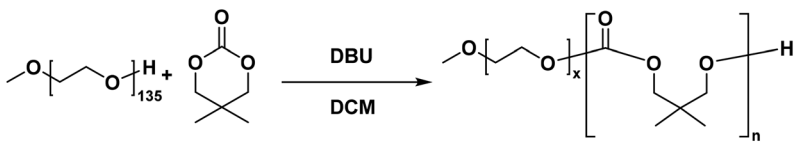

PEG_{135} DTC $PDTC_n$-*b*-PEG_x

Block polymer	PDTC DP_n [a]	M_n [b] (g mol^{-1})	$Đ_m$ [b]	PDTC : PEG block ratio[a]
$PDTC_{10}$-*b*-PEG_{124}	10	7770	1.05	1 : 12
$PDTC_{16}$-*b*-PEG_{129}	16	9600	1.07	1 : 8
$PDTC_{28}$-*b*-PEG_{130}	28	11 750	1.07	1 : 5
$PDTC_{49}$-*b*-PEG_{130}	49	13 700	1.06	1 : 3
$PDTC_{92}$-*b*-PEG_{132}	92	20 310	1.06	1 : 1

[a] Determined by ^{1}H NMR spectroscopy. [b] Determined by GPC *versus* polystyrene standards.

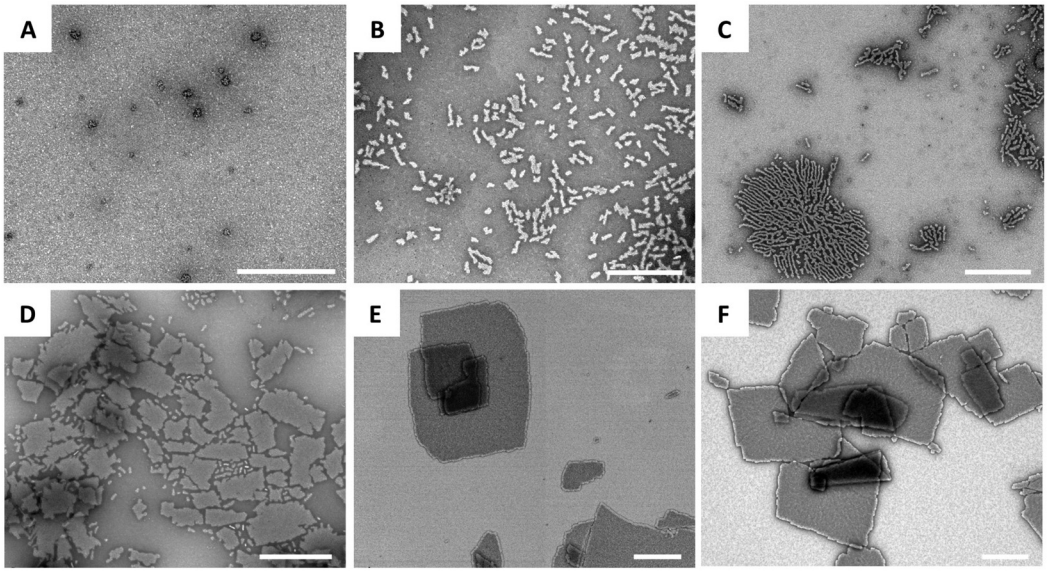

Fig. 2 TEM images of micelles prepared *via* homogeneous nucleation in MeOH : THF (v : v) 85 : 15 at 0.5 mg mL^{-1} by heating polymer samples to 70 °C for 2 h before cooling to 23 °C over a period of 2 h and aging over 24 h. (A) $PDTC_{10}$-*b*-PEG_{124}. (B) $PDTC_{16}$-*b*-PEG_{129}. (C) $PDTC_{28}$-*b*-PEG_{130}. (D) $PDTC_{49}$-*b*-PEG_{130}. (E) $PDTC_{92}$-*b*-PEG_{132}. (F) $PDTC_{92}$-*b*-PEG_{132} (MeOH : THF (v : v) 95 : 5). Scale bars = 500 nm. TEM images were obtained with uranyl acetate staining (3 wt% in MeOH).

of THF acts as a common solvent for both blocks to promote PDTC and PDEC crystallization.[22] The solutions for homogeneous nucleation experiments were prepared at 0.5 mg mL^{-1} in 85 : 15 MeOH : THF (v : v). The resulting solutions were drop-cast onto carbon coated copper grids and stained with uranyl acetate (3 wt% in MeOH) for transmission electron microscopy (TEM) analysis. Uranyl acetate stain was used to increase the contrast of low electron density $PDTC_m$-*b*-PEG_n- and $PDEC_m$-*b*-PEG_n-micelles relative to the carbon film, allowing better visualization of the nanostructures. As a result, the micelle core appears bright against the dark background as uranyl acetate only penetrates the PEG-corona but not the PDTC and PDEC micelle cores, repsectively.[50] As shown in Fig. 2, the morphologies of the resulting micelles prepared from the $PDTC_m$-*b*-PEG_n BCPs exhibited a clear transition from spherical micelles to 1D nanofibers, to 2D platelets as core-to-corona ratios increased. For example, $PDTC_{10}$-*b*-PEG_{124} with the lowest core-to-corona ratio of 1 : 12 formed spherical micelles with a diameter of *ca.* 28 nm (Fig. 2A). However, short nanofibers (*ca.* 76 and 127 nm) were observed for $PDTC_{16}$-*b*-PEG_{129} and $PDTC_{28}$-*b*-PEG_{130} with core-to-corona ratios of 1 : 8 and 1 : 5, respectively (Fig. 2B and C). A further increase of the core-to-corona ratio to 1 : 3 and 1 : 1 for $PDTC_{49}$-*b*-PEG_{130} and $PDTC_{92}$-*b*-PEG_{132} yielded 2D platelets (Fig. 2D–F). Such morphological transition can be qualitatively explained by the chain packing theory proposed by Vilgis and Halperin,[63] which means a decrease in crowding of the tethered PEG corona due to the increased length of the PDTC core block will result in a less curved core–corona interface. This phenomenon is consistent with the self-assembly results of other crystalline–coil BCPs.[19,20,64] The resulting micelles prepared from the $PDEC_m$-*b*-PEG_n BCPs exhibited a similar transition from spherical micelles to 1D nanofibers, to 2D nanoribbons as the core-to-corona ratio increased (Fig. S24†). Notably, the 2D nanoribbons of $PDEC_{95}$-*b*-PEG_{98} exhibit higher aspect ratios than the 2D platelets of the PDTC analogue. However, due to unfavorable properties such as self-nucleation (Fig. S24C and D†) and poor colloidal stability (Fig. S25†), these BCPs were not further studied. Next, the height of 2D platelets formed by $PDTC_{92}$-*b*-PEG_{132} was analyzed by atomic force microscopy (AFM) revealing them to be flat and uniform with a height of *ca.* 8 nm (Fig. S26A†). By dividing the height of the micelle by the average chain length of the PDTC core, the amount of chain folds can be calculated. In its lowest energy helical conformation, two repeating units of PDTC exhibit a length of 0.95 nm.[65] This reveals an average unit length of 0.475 nm per monomer. This corresponds to an average chain length for the $PDTC_{92}$-core of *ca.* 43.7 nm, which is approximately five times the height of the micelle core, suggesting that it undergoes 4 chain folds. Additionally, X-ray diffraction (XRD) measurements revealed the crystalline nature of these 2D platelets (Fig. S26B†).[64]

Living CDSA of $PDTC_{92}$-*b*-PEG_{132} block copolymers

After the successful preparation of 2D platelets *via* CDSA, living CDSA (seeded-growth) was employed to fabricate 2D platelets of precisely controlled size (Fig. 3A). Seed platelets were prepared by sonication of disperse 2D platelets derived from a $PDTC_{92}$-*b*-PEG_{132} solution (0.5 mg mL^{-1} in 95 : 5 MeOH : THF) for 3 h at 0 °C. TEM analysis revealed seed micelles with a number-average area (A_n) of 0.51 × 10^4 nm^2 and low area dispersity ($Đ_A$ = 1.22) (Fig. S27†). As we have pre-

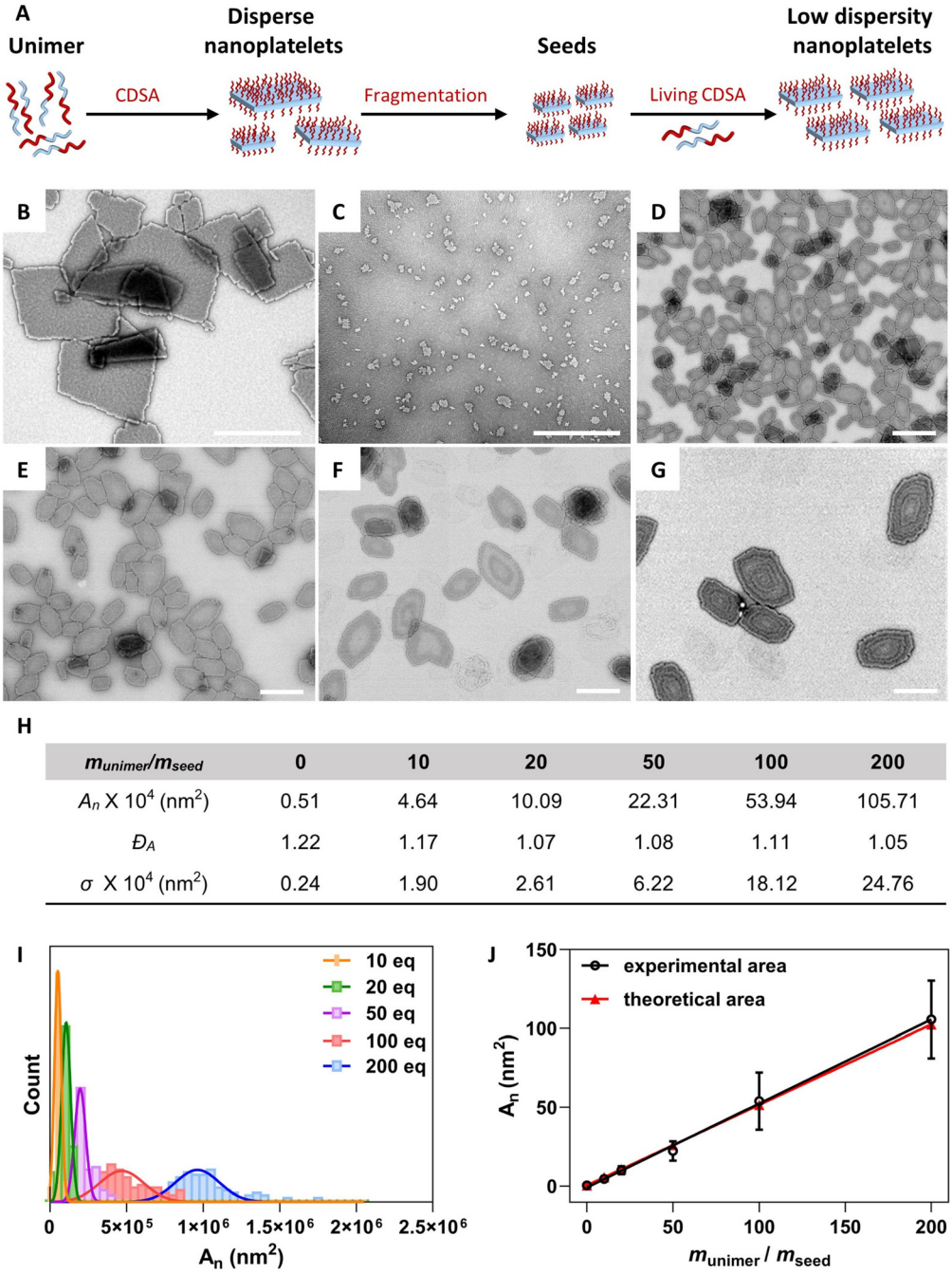

H

m_{unimer}/m_{seed}	0	10	20	50	100	200
A_n X 10^4 (nm^2)	0.51	4.64	10.09	22.31	53.94	105.71
$Đ_A$	1.22	1.17	1.07	1.08	1.11	1.05
σ X 10^4 (nm^2)	0.24	1.90	2.61	6.22	18.12	24.76

Fig. 3 Preparation of low dispersity platelets of controlled size by living CDSA. (A) Schematic representation of the preparation process of low dispersity 2D platelets from $PDTC_{92}$-*b*-PEG_{132}. (B) TEM micrograph of disperse platelets prepared in MeOH : THF (95 : 5) by homogeneous nucleation. (C) TEM image of seed platelets prepared by sonication of disperse platelets. TEM images of low dispersity platelets prepared through seeded-growth by addition of the unimer in THF to the platelet seed solution with a m_{unimer}/m_{seed} ratio of (D) 20 : 1, (E) 50 : 1, (F) 100 : 1 and (G) 200 : 1, respectively. Scale bars = 1 μm. TEM images were obtained with uranyl acetate staining (3 wt% in MeOH). (H) Summary of platelet area. $Đ_A$ is the area dispersity of the platelets. σ is the standard deviation of the area distribution. (I) Contour area histograms of low dispersity 2D platelets. (J) The plot of the experimental and theoretical A_n *versus* m_{unimer}/m_{seed}.

viously shown, the temperature significantly impacts the living CSDA (seeded growth) process as it influences the rate of crystallization and suppresses unimer aggregation.[20,66,67] Therefore, the effect of temperature on the seeded growth process of 2D platelet seeds of $PDTC_{92}$-*b*-PEG_{132} was evaluated. For this, seed micelles were kept at three different temperatures (23, 30 and 40 °C), while the same amount of unimer solution in THF with a unimer-to-seed mass ratio (m_{unimer}/m_{seed}) of 20 : 1 was added to each sample. The resulting 2D platelets are of different size and uniformity (Fig. S28†). The

2D platelets obtained after preheating the seeds at 40 °C are of the expected area, suggesting effective suppression of unimer aggregation at elevated temperatures (Fig. S28C†). Next, area control of 2D platelets was employed by varying the m_{unimer}/m_{seed} ratio at elevated temperatures. Different amounts of unimer solution of $PDTC_{92}$-*b*-PEG_{132} in THF (10 mg mL^{-1}) were added to the preformed seed micelle solutions at 40 °C. Low-area-dispersity 2D platelets were formed with controllable areas up to 105.71 × 10^4 nm^2, as shown by TEM (Fig. 3D–G). An excellent linear relationship between the resulting micelle area and the m_{unimer}/m_{seed} consistent with the expected theoretical area was observed (Fig. 3H–J), confirming the living CDSA behavior of $PDTC_{92}$-*b*-PEG_{132}. This represents a rare example of uniform and exceptionally well-controlled biodegradable 2D platelets from the seeded-growth of a 2D seed.

Triblock comicelles prepared by sequential living CDSA

To illustrate their potential as building blocks for hierarchical assembly, triblock comicelles with distinct coronal segments were prepared by the sequential addition of BCPs with different coronal chemistries to preformed 2D platelets (Fig. 4A). To achieve this, a PDTC-based BCP with a poly(2-vinylpyridine) (P2VP) corona block was prepared by a combination of ROP and reversible addition–fragmentation transfer (RAFT) polymerization. The DP_n of each block was identified by ^1H NMR spectroscopy and GPC analysis revealed low dispersity ($Đ_m$) values of 1.10 for $PDTC_{128}$-*b*-$P2VP_{61}$ (Fig. S29†). Due to the good solubility of both PEG and P2VP corona-segments in MeOH, it was anticipated that block comicelles could be prepared by adding the $PDTC_{128}$-*b*-$P2VP_{61}$ unimer to preformed $PDTC_{92}$-*b*-PEG_{132} platelets in MeOH. Briefly, the $PDTC_{128}$-*b*-$P2VP_{61}$ unimer (10 mg mL^{-1} in THF) was added to preformed $PDTC_{92}$-*b*-PEG_{132} low dispersity 2D platelets (A_n = 10.09 × 10^4 nm^2, $Đ_A$ = 1.07), resulting in uniform AB core–shell block 2D platelets (A_n = 45.58 × 10^4 nm^2, $Đ_A$ = 1.07) (Fig. 4B, Fig. S30A and B†). TEM analysis of the dropcast and negatively stained samples showed two clearly defined segments, due to the higher electron contrast of the outer segment P2VP corona than that of the inner segment PEG corona.

In addition, the use of fluorescent dye labeled BCPs allows micelle morphologies to be studied *in situ* using confocal laser scanning microscopy (CLSM). Therefore, fluorescent-dye labeled $PDTC_{92}$-*b*-PEG_{132}-Dy was prepared by the condensation of a carboxylic acid functionalized BODIPY-FL dye with the hydroxy chain end of the PDTC core segment. The attachment of the fluorescent dye was confirmed by UV-vis spectroscopy revealing the appearance of a strong absorbance band at 500 nm after dye functionalization (Fig. S31†). Further addition of the dye functionalized $PDTC_{92}$-*b*-PEG_{132}-Dy unimer (10 mg mL^{-1} in THF) to the preformed AB core–shell block 2D platelets yielded uniform ABC three-layer 2D platelets (A_n = 66.79 × 10^4 nm^2, $Đ_A$ = 1.08) as revealed by TEM (Fig. 4C and Fig. S30C†). The outermost fluorescent layer was confirmed with CLSM, which appears to be hollow 2D platelets (Fig. 4D).

Aqueous stability and compatibility of $PDTC_{92}$-*b*-PEG_{135} 2D platelets

To explore the biocompatibility of the prepared 2D platelets, their aqueous stability and cytotoxicity were evaluated. A sample of uniform 2D platelets (BCP = $PDTC_{92}$-*b*-PEG_{132}, A_n = 4.02 × 10^4 nm^2, $Đ_A$ = 1.13) was prepared at a concentration of 2 mg mL^{-1} (Fig. 5A and Fig. S32A†). The aqueous colloidal stability of these 2D platelets was explored by dialysis against water. This resulted in a clear, colloidally stable solution with

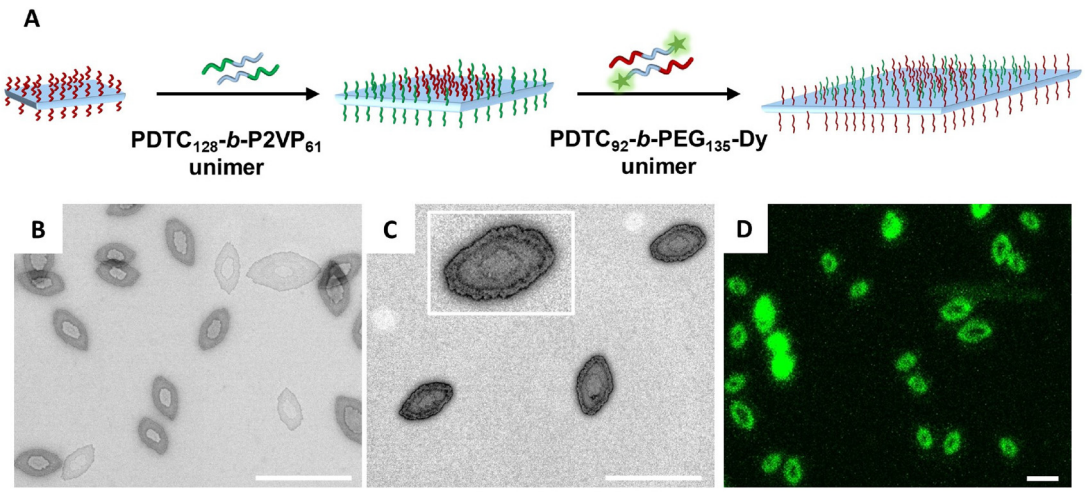

Fig. 4 (A) Schematic representation of the preparation process of uniform triblock comicelles by sequential living CDSA steps of preformed 2D platelets of $PDTC_{92}$-*b*-PEG_{132}. The PDTC core is depicted in blue, the PEG corona in red, the P2VP corona in green and the BODIPY-FL dye as green stars. (B) TEM image of PEG-*b*-P2VP block comicelles prepared from $PDTC_{92}$-*b*-PEG_{132} platelets (A_n = 10.09 × 10^4 nm^2, $Đ_A$ = 1.07) and $PDTC_{128}$-*b*-$P2VP_{61}$ unimers. (C) TEM image of PEG-*b*-P2VP-*b*-PEG-Dy triblock comicelles prepared from the resulting block comicelles and $PDTC_{92}$-*b*-PEG_{132}-Dy unimers. Magnified TEM image of a triblock comicelle. (D) CLSM images of the three-layer 2D platelets. Scale bars = 2 μm. TEM images were obtained with uranyl acetate staining (3 wt% in MeOH), Dy = BODIPY-FL.

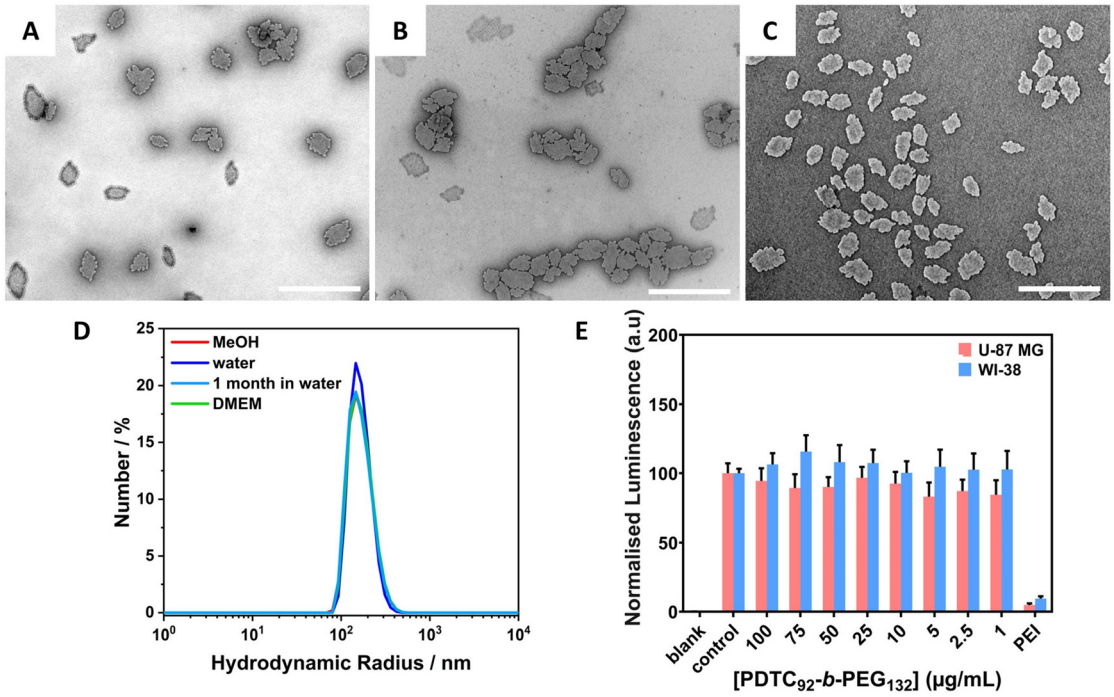

Fig. 5 (A) TEM image of $PDTC_{92}$-*b*-PEG_{132} platelets before dialysis from MeOH into water. (B) TEM image of $PDTC_{92}$-*b*-PEG_{132} platelets after dialysis. Platelets are in proximity due to a drying effect on the carbon coated TEM grid. (C) TEM of $PDTC_{92}$-*b*-PEG_{132} in water after 1 month of storage. Scale bars = 1 μm. TEM images were obtained with uranyl acetate staining (3 wt% in MeOH). (D) R_h of 2D platelet micelles before and after dialysis, stored in water for one month and in DMEM cell culture media. (E) Cell viability was measured after 24 h exposure of WI-38 and U-87 MG cells to different concentrations of 2D platelet micelles (A_n = 3.85 × 10^4 nm^2, $Đ_A$ = 1.14) in water.

no observable change in the micelle morphology *via* TEM analysis (A_n = 3.85 × 10^4 nm^2, $Đ_A$ = 1.14) (Fig. 5B and Fig. S32B†). Dynamic light scattering (DLS) experiments revealed no change in the hydrodynamic radius (R_h *ca.* 200 nm) after solvent exchange from MeOH to water (Fig. 5C). To assess the colloidal stability of the 2D platelets in water over time, TEM and DLS analyses were performed on 2D platelets stored in water for 1 month, which revealed negligible changes in size and dispersity (Fig. 5B, C and Fig. S32C†). These results confirmed the excellent stability of the uniform 2D platelets in aqueous media and allowed further examination of the potential biocompatibility of these platelets. For this, the preformed 2D platelets were diluted in Dulbecco's modified Eagle's medium (DMEM) and no changes in the hydrodynamic radius were revealed by DLS (Fig. 5D). WI-38 fetal lung fibroblasts and U-87 MG glioblastoma cells were incubated with the preformed 2D platelets at concentrations ranging from 1 to 100 μg mL^{-1}. The analysis of the cell populations showed that 2D platelets of $PDTC_{92}$-*b*-PEG_{132} exhibit no discernible cytotoxicity towards either cell line (Fig. 5E and Table S3†). These results reveal excellent biocompatibility, similar to PFTMC-based nanomaterials; however, the cytotoxicity of the PFTMC-biodegradation product is of concern. Therefore, the biocompatibility of the hydrolytic biodegradation product of PDTC, 2,2-dimethylpropane-1,3-diol, was evaluated in both cell lines (Fig. S33 and Table S4†).[42,43] The biodegradation product exhibits no discernible cytotoxicity towards either cell line up to a concentration of 250 μg mL^{-1} proving that PDTC-based BCPs form less harmful biodegradation products in comparison with PFTMC-based BCPs.

Conclusions

In summary, we have developed a series of crystalline aliphatic polycarbonates through the introduction of different side chains and cyclic side groups to PTMC. The dimethyl substituted polycarbonate PDTC was selected as a core-forming block due to its improved crystallinity, compared to other PTMC derivatives. By harnessing the living CDSA of $PDTC_{92}$-*b*-PEG_{132}, we were able to access uniform 2D platelets and segmented triblock comicelles with controlled size and spatially defined corona compositions. The core-forming block undergoes exceptionally well-controlled living CDSA from 2D seeds in contrast to other biodegradable cores. This represents the first example of size controlled 2D platelets from a BCP with a crystalline polycarbonate-based core-forming block. More importantly, these synthetic 2D platelets exhibit great colloidal stability in aqueous solutions and excellent biocompatibility. Next, we were able to show that PDTC forms less harmful degradation products than PFTMC revealing its enhanced biocompatibility. Future work will focus on applying these 2D platelets with tailored corona chemistries in biomedical applications.

Author contributions

Hannah Schnicke: conceptualization (supporting), formal analysis (supporting), investigation, visualization, and writing – review & editing (lead). Chuanqi Zhao: conceptualization (lead), formal analysis (lead), investigation, methodology, visualization, and writing – original draft. J. Diego Garcia-Hernandez: methodology (monomer synthesis). Jiandong Cai: visualization (AFM and CLSM imaging). Yifan Zhang: conceptualization (triblock comicelles). Charlotte E. Boott: writing – review and editing. Ian Manners: conceptualization, funding acquisition, resources, supervision, and writing – review and editing.

Conflicts of interest

The authors declare no competing financial interests.

Acknowledgements

The work was funded by the Canada 150 Research Chair supported by the Canadian Government and NSERC Discovery Grants (to I. M). I. M. also thanks the University of Victoria for start-up funds and the Canada Foundation for Innovation (CFI), the British Columbia Knowledge Development Fund (BCKDF), and NSERC for equipment and instrumentational support.

References

1 C. Yang, Z. X. Li and J. T. Xu, Single crystals and two-dimensional crystalline assembliesof block copolymers, *J. Polym. Sci.*, 2022, **60**(15), 2153–2174. Available from: https://onlinelibrary.wiley.com/doi/epdf/10.1002/pol.20210866.

2 B. Dong, D. L. Miller and C. Y. Li, Polymer Single Crystal as Magnetically Recoverable Support for Nanocatalysts, *J. Phys. Chem. Lett.*, 2012, **3**(10), 1346–1350, DOI: 10.1021/jz300434c.

3 Z. Wang, Q. Jingjing, X. Wang, Z. Zhang, Y. Chen, X. Huang and W. Huang, Two-Dimensional Light-Emitting Materials: Preparation, Properties and Applications, *Chem. Soc. Rev.*, 2018, **47**(16), 6128–6174, DOI: 10.1039/C8CS00332G.

4 S. Lei, J. Tian, Y. Kang, Y. Zhang and I. Manners, AIE-Active, Stimuli-Responsive Fluorescent 2D Block Copolymer Nanoplatelets Based on Corona Chain Compression, *J. Am. Chem. Soc.*, 2022, **144**(38), 17630–17641, DOI: 10.1021/jacs.2c07133.

5 Y. Gong, L. Fu, Y. Che, H. Ji, Y. Zhang, L. Zang, J. Zhao and Y. Che, *J. Am. Chem. Soc.*, 2023, **145**(17), 9771–9776, DOI: 10.1021/jacs.3c01517.

6 L. Han, H. Fan, Y. Zhu, M. Wang, F. Pan, D. Yu, Y. Zhao and F. He, Precisely Controlled Two-Dimensional Rhombic Copolymer Micelles for Sensitive Flexible Tunneling Devices, *CCS Chem.*, 2021, **3**(5), 1399–1409, DOI: 10.31635/ccschem.020.202000297.

7 S. Yang, S. Shin, I. Choi, J. Lee and T. L. Choi, Direct Formation of Large-Area 2D Nanosheets from Fluorescent Semiconducting Homopolymer with Orthorhombic Crystalline Orientation, *J. Am. Chem. Soc.*, 2017, **139**(8), 3082–3088, DOI: 10.1021/jacs.6b12378.

8 A. Rajak and A. Das, Crystallization-Driven Controlled Two-Dimensional (2D) Assemblies from Chromophore-Appended Poly(L-Lactide)s: Highly Efficient Energy Transfer on a 2D Surface, *Angew. Chem., Int. Ed.*, 2022, **61**(15), e202116572, DOI: 10.1002/anie.202116572.

9 N. Rohaizad, C. C. Mayorga-Martinez, M. Fojtů, N. M. Latiff and M. Pumera, Two-Dimensional Materials in Biomedical, Biosensing and Sensing Applications, *Chem. Soc. Rev.*, 2021, **50**(1), 619–657, DOI: 10.1039/d0cs00150c.

10 Y. Song, M. Elsabahy, C. A. Collins, S. Khan, R. Li, T. N. Hreha, Y. Shen, Y. N. Lin, R. A. Letteri, L. Su, M. Dong, F. Zhang, D. A. Hunstad and K. L. Wooley, Morphologic Design of Silver-Bearing Sugar-Based Polymer Nanoparticles for Uroepithelial Cell Binding and Antimicrobial Delivery, *Nano Lett.*, 2021, **21**(12), 4990–4998, DOI: 10.1021/acs.nanolett.1c00776.

11 S. Ganda, C. K. Wong, J. Biazik, R. Raveendran, L. Zhang, F. Chen, N. Ariotti and M. H. Stenzel, Macrophage-Targeting and Complete Lysosomal Degradation of Self-Assembled Two-Dimensional Poly(ε-Caprolactone) Platelet Particles, *ACS Appl. Mater. Interfaces*, 2022, **14**(31), 35333–35343, DOI: 10.1021/acsami.2c06555.

12 S. Muro, C. Garnacho, J. A. Champion, J. Leferovich, C. Gajewski, E. H. Schuchman, S. Mitragotri and V. R. Muzykantov, Control of Endothelial Targeting and Intracellular Delivery of Therapeutic Enzymes by Modulating the Size and Shape of ICAM-1-Targeted Carriers, *Mol. Ther.*, 2008, **16**(8), 1450–1458, DOI: 10.1038/mt.2008.127.

13 Z. Li, Y. Zhang, L. Wu, W. Yu, T. R. Wilks, A. P. Dove, H. M. Ding, R. K. O'Reilly, G. Chen and M. Jiang, Glyco-Platelets with Controlled Morphologies via Crystallization-Driven Self-Assembly and Their Shape-Dependent Interplay with Macrophages, *ACS Macro Lett.*, 2019, **8**(5), 596–602, DOI: 10.1021/acsmacrolett.9b00221.

14 X. Zhang, G. Chen, B. Zheng, Z. Wan, L. Liu, L. Zhu, Y. Xie and Z. Tong, Uniform Two-Dimensional Crystalline Platelets with Tailored Compositions for PH Stimulus-Responsive Drug Release, *Biomacromolecules*, 2023, **24**(2), 1032–1041, DOI: 10.1021/acs.biomac.2c01481.

15 J. T. Lovegrove, R. Raveendran, P. Spicer, S. Förster, C. J. Garvey and M. H. Stenzel, Margination of 2D Platelet Microparticles in Blood, *ACS Macro Lett.*, 2023, **12**(3), 344–349, DOI: 10.1021/acsmacrolett.2c00718.

16 A. K. Pearce, T. R. Wilks, M. C. Arno and R. K. O'Reilly, Synthesis and Applications of Anisotropic Nanoparticles with Precisely Defined Dimensions, *Nat. Rev. Chem.*, 2021, **5**(1), 21–45, DOI: 10.1038/s41570-020-00232-7.

17 U. Tritschler, S. Pearce, J. Gwyther, G. R. Whittell and I. Manners, 50th Anniversary Perspective: Functional Nanoparticles from the Solution Self-Assembly of Block Copolymers, *Macromolecules*, 2017, **50**(9), 3439–3463, DOI: 10.1021/acs.macromol.6b02767.

18 X. He, M. S. Hsiao, C. E. Boott, R. L. Harniman, A. Nazemi, X. Li, M. A. Winnik and I. Manners, Two-Dimensional Assemblies from Crystallizable Homopolymers with Charged Termini, *Nat. Mater.*, 2017, **16**(4), 481–488, DOI: 10.1038/nmat4837.

19 Z. M. Hudson, C. E. Boott, M. E. Robinson, P. A. Rupar, M. A. Winnik and I. Manners, Tailored Hierarchical Micelle Architectures Using Living Crystallization-Driven Self-Assembly in Two Dimensions, *Nat. Chem.*, 2014, **6**(10), 893–898, DOI: 10.1038/nchem.2038.

20 X. Zhang, G. Chen, L. Liu, L. Zhu and Z. Tong, Precise Control of Two-Dimensional Platelet Micelles from Biodegradable Poly(p-Dioxanone) Block Copolymers by Crystallization-Driven Self-Assembly, *Macromolecules*, 2022, **55**(18), 8250–8261, DOI: 10.1021/acs.macromol.2c01158.

21 R. A. Scanga, A. Shahrokhinia, J. Borges, S. H. Sarault, M. B. Ross and J. F. Reuther, Asymmetric Polymerization-Induced Crystallization-Driven Self-Assembly of Helical, Rod-Coil Poly(Aryl Isocyanide) Block Copolymers, *J. Am. Chem. Soc.*, 2023, **145**(11), 6319–6329, DOI: 10.1021/jacs.2c13354.

22 M. S. Hsiao, S. F. M. Yusoff, M. A. Winnik and I. Manners, Crystallization-Driven Self-Assembly of Block Copolymers with a Short Crystallizable Core-Forming Segment: Controlling Micelle Morphology through the Influence of Molar Mass and Solvent Selectivity, *Macromolecules*, 2014, **47**(7), 2361–2372, DOI: 10.1021/ma402429d.

23 S. Song, Q. Yu, H. Zhou, G. Hicks, H. Zhu, C. K. Rastogi, I. Manners and M. A. Winnik, Solvent Effects Leading to a Variety of Different 2D Structures in the Self-Assembly of a Crystalline-Coil Block Copolymer with an Amphiphilic Corona-Forming Block, *Chem. Sci.*, 2020, **11**(18), 4631–4643, DOI: 10.1039/d0sc01453b.

24 M. Inam, G. Cambridge, A. Pitto-Barry, Z. P. L. Laker, N. R. Wilson, R. T. Mathers, A. P. Dove and R. K. O'Reilly, 1D vs. 2D Shape Selectivity in the Crystallization-Driven Self-Assembly of Polylactide Block Copolymers, *Chem. Sci.*, 2017, **8**(6), 4223–4230, DOI: 10.1039/C7SC00641A.

25 W. Yu, M. Inam, J. R. Jones, A. P. Dove and R. K. O'Reilly, Understanding the CDSA of Poly(Lactide) Containing Triblock Copolymers, *Polym. Chem.*, 2017, **8**(36), 5504–5512, DOI: 10.1039/C7PY01056G.

26 M. C. Arno, M. Inam, Z. Coe, G. Cambridge, L. J. Macdougall, R. Keogh, A. P. Dove and R. K. O'Reilly, Precision Epitaxy for Aqueous 1D and 2D Poly(ε-Caprolactone) Assemblies, *J. Am. Chem. Soc.*, 2017, **139**(46), 16980–16985, DOI: 10.1021/jacs.7b10199.

27 Y. He, J. C. Eloi, R. L. Harniman, R. M. Richardson, G. R. Whittell, R. T. Mathers, A. P. Dove, R. K. O'Reilly and I. Manners, Uniform Biodegradable Fiber-Like Micelles and Block Comicelles via "Living" Crystallization-Driven Self-Assembly of Poly(l-Lactide) Block Copolymers: The Importance of Reducing Unimer Self-Nucleation via Hydrogen Bond Disruption, *J. Am. Chem. Soc.*, 2019, **141**(48), 19088–19098, DOI: 10.1021/jacs.9b09885.

28 X. Wang, G. Guerin, H. Wang, Y. Wang, I. Manners and M. A. Winnik, Cylindrical Block Copolymer Micelles and Co-Micelles of Controlled Length and Architecture, *Science*, 2007, **317**(5838), 644–647, DOI: 10.1126/science.1141382.

29 J. Schmelz, A. E. Schedl, C. Steinlein, I. Manners and H. Schmalz, Length Control and Block-Type Architectures in Worm-like Micelles with Polyethylene Cores, *J. Am. Chem. Soc.*, 2012, **134**(34), 14217–14225, DOI: 10.1021/ja306264d.

30 S. Ganda and M. H. Stenzel, Concepts, Fabrication Methods and Applications of Living Crystallization-Driven Self-Assembly of Block Copolymers, *Prog. Polym. Sci.*, 2020, **101**, 101195, DOI: 10.1016/j.progpolymsci.2019.101195.

31 J. B. Gilroy, T. Gädt, G. R. Whittell, L. Chabanne, J. M. Mitchels, R. M. Richardson, M. A. Winnik and I. Manners, Monodisperse Cylindrical Micelles by Crystallization-Driven Living Self-Assembly, *Nat. Chem.*, 2010, **2**(7), 566–570, DOI: 10.1038/nchem.664.

32 J. R. Finnegan, T. P. Davis and K. Kempe, Heat-Induced Living Crystallization-Driven Self-Assembly: The Effect of Temperature and Polymer Composition on the Assembly and Disassembly of Poly(2-Oxazoline) Nanorods, *Macromolecules*, 2022, **55**(9), 3650–3660, DOI: 10.1021/acs.macromol.2c00298.

33 L. MacFarlane, C. Zhao, J. Cai, H. Qiu and I. Manners, Emerging Applications for Living Crystallization-Driven Self-Assembly, *Chem. Sci.*, 2021, **12**(13), 4661–4682, DOI: 10.1039/d0sc06878k.

34 S. Ganda, C. K. Wong and M. H. Stenzel, Corona-Loading Strategies for Crystalline Particles Made by Living Crystallization-Driven Self-Assembly, *Macromolecules*, 2021, **54**(14), 6662–6669, DOI: 10.1021/acs.macromol.1c00643.

35 X. He, Y. He, M. S. Hsiao, R. L. Harniman, S. Pearce, M. A. Winnik and I. Manners, Complex and Hierarchical 2D Assemblies via Crystallization-Driven Self-Assembly of Poly(l -Lactide) Homopolymers with Charged Termini, *J. Am. Chem. Soc.*, 2017, **139**(27), 9221–9228, DOI: 10.1021/jacs.7b03172.

36 M. Inam, J. R. Jones, M. M. Pérez-Madrigal, M. C. Arno, A. P. Dove and R. K. O'Reilly, Controlling the Size of Two-Dimensional Polymer Platelets for Water-in-Water Emulsifiers, *ACS Cent. Sci.*, 2017, **4**(1), 63–70, DOI: 10.1021/acscentsci.7b00436.

37 C. Zhu and J. Nicolas, (Bio)Degradable and Biocompatible Nano-Objects from Polymerization-Induced and Crystallization-Driven Self-Assembly, *Biomacromolecules*, 2022, **23**(8), 3043–3080, DOI: 10.1021/acs.biomac.2c00230.

38 T. Xia, Z. Tong, Y. Xie, M. C. Arno, S. Lei, L. Xiao, J. Y. Rho, C. T. Y. Ferguson, I. Manners, A. P. Dove and R. K. O'Reilly, Tuning the Functionality of Self-Assembled 2D Platelets in the Third Dimension, *J. Am. Chem. Soc.*, 2023, **145**(46), 24274–25282, DOI: 10.1021/jacs.3c08770.

39 Z. Tong, Y. Xie, M. C. Arno, Y. Zhang, I. Manners, R. K. O'Reilly and A. P. Dove, Uniform segmented platelet micelles with compositionally distinct and selectively degradable cores, *Nat. Chem.*, 2023, **15**, 824–831. Available from: https://www.nature.com/articles/s41557-023-01177-2.

40 L. Xiao, S. J. Parkinson, T. Xia, P. Edge and R. K. O'Reilly, *ACS Macro Lett.*, 2023, **12**(12), 1636–1641, DOI: 10.1021/acsmacrolett.3c00600.

41 Y. Xie, Z. Tong, T. Xia, J. C. Worch, J. Y. Rho, A. P. Dove and R. K. O'Reilly, *Adv. Mater.*, 2024, **36**(8), 2308154, DOI: 10.1002/adma.202308154.

42 W. Yu, E. Maynard, V. Chiaradia, M. C. Arno and A. P. Dove, Aliphatic Polycarbonates from Cyclic Carbonate Monomers and Their Application as Biomaterials, *Chem. Rev.*, 2021, **121**(18), 10865–10907, DOI: 10.1021/acs.chemrev.0c00883.

43 R. P. Brannigan and A. P. Dove, Synthesis, Properties and Biomedical Applications of Hydrolytically Degradable Materials Based on Aliphatic Polyesters and Polycarbonates, *Biomater. Sci.*, 2016, **5**(1), 9–21, DOI: 10.1039/c6bm00584e.

44 Z. Zhang, R. Kuijer, S. K. Bulstra, D. W. Grijpma and J. Feijen, The in Vivo and in Vitro Degradation Behavior of Poly(Trimethylene Carbonate), *Biomaterials*, 2006, **27**(9), 1741–1748, DOI: 10.1016/j.biomaterials.2005.09.017.

45 F. Nederberg, Y. Zhang, J. P. K. Tan, K. Xu, H. Wang, C. Yang, S. Gao, X. D. Guo, K. Fukushima, L. Li, J. L. Hedrick and Y. Y. Yang, Biodegradable Nanostructures with Selective Lysis of Microbial Membranes, *Nat. Chem.*, 2011, **3**(5), 409–414, DOI: 10.1038/nchem.1012.

46 K. Fukushima, Poly(Trimethylene Carbonate)-Based Polymers Engineered for Biodegradable Functional Biomaterials, *Biomater. Sci.*, 2016, **4**(1), 9–24, DOI: 10.1039/c5bm00123d.

47 A. P. Pêgo, D. W. Grijpma and J. Feijen, Enhanced Mechanical Properties of 1,3-Trimethylene Carbonate Polymers and Networks, *Polymer*, 2003, **44**(21), 6495–6504, DOI: 10.1016/S0032-3861(03)00668-2.

48 L. W. Yang, B. He, S. Meng, J. Z. Zhang, M. Li, J. Guo, Y. M. Guan, J. X. Li and Z. W. Gu, Biodegradable cross-linked poly(trimethylene carbonate) networks for implant applications: Synthesis and properties, *Polymer*, 2013, **54**(11), 2668–2675, DOI: 10.1016/j.polymer.2013.03.059.

49 Y. Takahashi and R. Kojima, Crystal Structure of Poly (Trimethylene Carbonate), *Macromolecules*, 2003, **36**(14), 5139–5143, DOI: 10.1021/ma030076q.

50 J. R. Finnegan, X. He, S. T. G. Street, J. D. Garcia-Hernandez, D. W. Hayward, R. L. Harniman, R. M. Richardson, G. R. Whittell and I. Manners, Extending the Scope of "Living" Crystallization-Driven Self-Assembly: Well-Defined 1D Micelles and Block Comicelles from Crystallizable Polycarbonate Block Copolymers, *J. Am. Chem. Soc.*, 2018, **140**(49), 17127–17140, DOI: 10.1021/jacs.8b09861.

51 R. N. L. Hailes, A. M. Oliver, J. Gwyther, G. R. Whittell and I. Manners, Polyferrocenylsilanes: synthesis, properties, and applications, *Chem. Soc. Rev.*, 2016, **45**(19), 5358–5407, DOI: 10.1039/C6CS00155F.

52 J. D. Garcia-Hernandez, S. T. G. Street, Y. Kang, Y. Zhang and I. Manners, Cargo Encapsulation in Uniform, Length-Tunable Aqueous Nanofibers with a Coaxial Crystalline and Amorphous Core, *Macromolecules*, 2021, **54**(12), 5784–5796, DOI: 10.1021/acs.macromol.1c00672.

53 C. E. Ellis, J. D. Garcia-Hernandez and I. Manners, Scalable and Uniform Length-Tunable Biodegradable Block Copolymer Nanofibers with a Polycarbonate Core via Living Polymerization-Induced Crystallization-Driven Self-Assembly, *J. Am. Chem. Soc.*, 2022, **144**(44), 20525–20538, DOI: 10.1021/jacs.2c09715.

54 C. Zhao, Q. Chen, J. D. Garcia-Hernandez, L. K. Watanabe, J. M. Rawson, J. Rao and I. Manners, Uniform and Length-Tunable, Paramagnetic Self-Assembled Nitroxide-Based Nanofibers for Magnetic Resonance Imaging, *Macromolecules*, 2023, **56**(1), 263–270, DOI: 10.1021/acs.macromol.2c02227.

55 S. T. G. Street, Y. He, L. Robert, R. L. Harniman, J. G. Garcia-Hernandez and I. Manners, Precision polymer nanofibers with a responsive polyelectrolyte corona designed as a modular, functionalizable nanomedicine platform, *Polym. Chem.*, 2022, **13**(20), 3009. Available from: https://pubs.rsc.org/en/content/articlelanding/2022/py/d2py00152g.

56 H. C. Parkin, J. D. Garcia-Hernandez, S. T. G. Street, R. Hof and I. Manners, Uniform, Length-Tunable Antibacterial 1D Diblock Copolymer Nanofibers, *Polym. Chem.*, 2022, **13**(20), 2941–2949, DOI: 10.1039/D2PY00262K.

57 H. C. Parkin, S. T. G. Street, B. Gowen, L. H. Da-Silva-Correa, R. Hof, H. L. Buckley and I. Manners, *J. Am. Chem. Soc.*, 2024, **146**(8), 5128–5141. Available from: https://pubs.acs.org/doi/full/10.1021/jacs.3c09033.

58 S. T. G. Street, J. Chrenek, R. L. Harniman, K. Letwin, J. M. Mantell, U. Boruc, S. M. Willerth and I. Manners, Length-Controlled Nanofiber Micelleplexes as Efficient Nucleic Acid Delivery Vehicles, *J. Am. Chem. Soc.*, 2022, **144**(43), 19799–19812, DOI: 10.1021/jacs.2c06695.

59 T. Gädt, F. H. Schacher, N. McGrath, M. S. Winnik and I. Manners, Probing the Scope of Crystallization-Driven Living Self-Assembly: Studies of Diblock Copolymer Micelles with a Polyisoprene Corona and a Crystalline Poly (ferrocenyldiethylsilane) Core-Forming Metalloblock, *Macromolecules*, 2011, **44**(10), 3777–3786. Available from: https://pubs.acs.org/doi/full/10.1021/ma1029289.

60 R. N. L. Hailes, A. M. Oliver, J. Gwyther, G. R. Whittell and I. Manners, *Chem. Soc. Rev.*, 2016, **45**(19), 5358–5407. Available from: https://pubs.rsc.org/en/content/articlelanding/2016/cs/c6cs00155f.

61 S. Song, H. Zhou, I. Manners and M. A. Winnik, Block Copolymer Self-Assembly: Polydisperse Corona-Forming Blocks Leading to Uniform Morphologies, *Chem*, 2021, **7**(10), 2800–2821, DOI: 10.1016/j.chempr.2021.08.003.

62 K. E. B. Doncom, L. D. Blackman, D. B. Wright, M. I. Gibson and R. K. O'Reilly, Dispersity Effects in

Polymer Self-Assemblies: A Matter of Hierarchical Control, *Chem. Soc. Rev.*, 2017, **46**(14), 4119–4134, DOI: **10.1039/c6cs00818f**.

63 T. Vilgis and A. Halperin, Aggregation of Coil-Crystalline Block Copolymers: Equilibrium Crystallization, *Macromolecules*, 1991, **24**(8), 2090–2095, DOI: **10.1021/ma00008a058**.

64 Z. Tong, Y. Li, H. Xu, H. Chen, W. Yu, W. Zhuo, R. Zhang and G. Jiang, Corona Liquid Crystalline Order Helps to Form Single Crystals When Self-Assembly Takes Place in the Crystalline/Liquid Crystalline Block Copolymers, *ACS Macro Lett.*, 2016, **5**(7), 867–872, DOI: **10.1021/acsmacrolett.6b00428**.

65 G. Sidoti, S. Capelli, S. V. Meille and G. C. Alfonso, The Polymorphic Behaviour of Poly(2,2-Dimethyltrimethylenecarbonate) and of Its Cyclic Monomer. Evidence for a High Entropy, Conformationally Disordered Modification, *Polymer*, 1998, **39**(1), 165–172, DOI: **10.1016/S0032-3861(97)00224-3**.

66 L. R. MacFarlane, X. Li, C. F. J. Faul and I. Manners, Efficient and Controlled Seeded Growth of Poly(3-Hexylthiophene) Block Copolymer Nanofibers through Suppression of Homogeneous Nucleation, *Macromolecules*, 2021, **54**(24), 11269–11280, DOI: **10.1021/acs.macromol.1c02005**.

67 D. Tao, C. Feng, Y. Cui, X. Yang, I. Manners, M. A. Winnik and X. Huang, Monodisperse Fiber-like Micelles of Controlled Length and Composition with an Oligo(p-Phenylenevinylene) Core via "Living" Crystallization-Driven Self-Assembly, *J. Am. Chem. Soc.*, 2017, **139**(21), 7136–7139, DOI: **10.1021/jacs.7b02208**.